

Local frequency dependence in transcranial ultrasound transmission

P J White, G T Clement and K Hynynen

Department of Radiology, Harvard Medical School, Brigham and Women's Hospital, Boston, MA 02115, USA

Received 6 October 2005, in final form 27 March 2006

Published 19 April 2006

Online at stacks.iop.org/PMB/51/2293

Abstract

The development of large-aperture multiple-source transducer arrays for ultrasound transmission through the human skull has demonstrated the possibility of controlled and substantial acoustic energy delivery into the brain parenchyma without the necessitation of a craniotomy. The individual control of acoustic parameters from each ultrasound source allows for the correction of distortions arising from transmission through the skull bone and also opens up the possibility for electronic steering of the acoustic focus within the brain. In addition, the capability to adjust the frequency of insonation at different locations on the skull can have an effect on ultrasound transmission. To determine the efficacy and applicability of a multiple-frequency approach with such a device, this study examined the frequency dependence of ultrasound transmission in the range of 0.6–1.4 MHz through a series of 17 points on four *ex vivo* human skulls. Effects beyond those that are characteristic of frequency-dependent attenuation were examined. Using broadband pulses, it was shown that the reflected spectra from the skull revealed information regarding ultrasound transmission at specific frequencies. A multiple-frequency insonation with optimized frequencies over the entirety of five skull specimens was found to yield on average a temporally brief 230% increase in the transmitted intensity with an 88% decrease in time-averaged intensity transmission within the focal volume. This finding demonstrates a potential applicability of a multiple-frequency approach in transcranial ultrasound transmission.

1. Introduction

The numerous suggested possibilities for applications of ultrasound within the brain include the treatment of brain tumours (Fry 1977, Hynynen and Jolesz 1998, Tanter *et al* 1998, Tobias *et al* 1987), targeted drug delivery (Hynynen *et al* 2001), thrombolytic stroke treatment (Behrens *et al* 2001), blood flow imaging (Kirkham *et al* 1986, Postert *et al* 2000) and tomographic brain imaging (Carson *et al* 1977, Dines *et al* 1981, Fry *et al* 1974, Smith *et al*

1979, Ylitalo *et al* 1990). While several of these applications have been suggested in conjunction with craniotomies, the exploration of transcranial ultrasound transmission has opened up the possibility of non-invasive procedures. The discovery in the early 1940s that high-intensity transcranial ultrasound generated an excessive amount of heating at the skull–tissue interface (Lynn *et al* 1942) became a challenge for ultrasound brain therapy research and led to the assumption that craniotomies were necessary for therapeutic ultrasound procedures in the brain.

More recently, several technologies and methodologies were studied and developed for improving the efficiency of ultrasound transmission through the skull bone; these have included the development of high-power large aperture transducers (Sun and Hynynen 1999), and the capability for controlled modulation of acoustic power and phase from multiple ultrasound sources (Daum *et al* 1998). The focused, large-aperture geometry of transcranial energy transmission minimized localized skull heating while the segmentation of transducers into individually controllable ultrasound sources provided a method to adaptively correct for phase and amplitude distortions.

Methods for the adaptive modulation of acoustic phase (Hynynen and Jolesz 1998) and amplitude (Thomas and Fink 1996) have been studied with the intention of reconstructing a desired ultrasound field given *a priori* knowledge of the Green's function for each source–target combination. These methods, however, were studied for single-frequency operation, precluding the consideration of localized frequency-dependent acoustic power transmission enhancement across the entire skull surface according to variation in both bone thickness and mass density.

The present study examined a method to select the most efficient frequency within a band of focal-gain-optimized frequencies (Clement *et al* 2000) for transmission through a localized portion of the human skull based on the backscatter pressure field from an applied acoustic impulse. A similar measurement methodology was previously performed, but for the purpose of predicting the phase shift caused by the skull at a given frequency (Aarnio *et al* 2005).

2. Materials and methods

2.1. Simulations

The theory of wave propagation in a fluid through an intermediary elastic layer has been described in detail in texts by Kinsler *et al* (1982) and Cheeke (2002), so only a brief outline of its pertinence to this study will be included. A detailed formulation for the transmission coefficient of a one-dimensional plane wave in a fluid medium, propagated through an intermediate solid elastic layer is presented in the appendix. This idealized transmission intensity coefficient,

$$T = \frac{1}{1 + \frac{1}{4} \left[\frac{(\rho c)_b}{(\rho c)_f} - \frac{(\rho c)_f}{(\rho c)_b} \right]^2 \sin^2 k_b d}, \quad (1)$$

and its associated reflection intensity coefficient,

$$\mathbf{R} = \frac{p_{rf}}{p_{if}} = \frac{j \left[\frac{(\rho c)_b}{(\rho c)_f} - \frac{(\rho c)_f}{(\rho c)_b} \right] \sin k_b d}{2 \cos k_b d + j \left[\frac{(\rho c)_b}{(\rho c)_f} + \frac{(\rho c)_f}{(\rho c)_b} \right] \sin k_b d}, \quad (2)$$

are shown in figure 1 for a 5 mm thick skull sample with parallel interfaces and a homogenous mass density cross-section ($\rho = 2450 \text{ kg m}^{-3}$, $c = 2650 \text{ m s}^{-1}$) submerged in water ($\rho = 1000 \text{ kg m}^{-3}$, $c = 1500 \text{ m s}^{-1}$). For this study, shear wave propagation through the skull is not considered since the impinging ultrasound propagation vectors are all normal to the surface

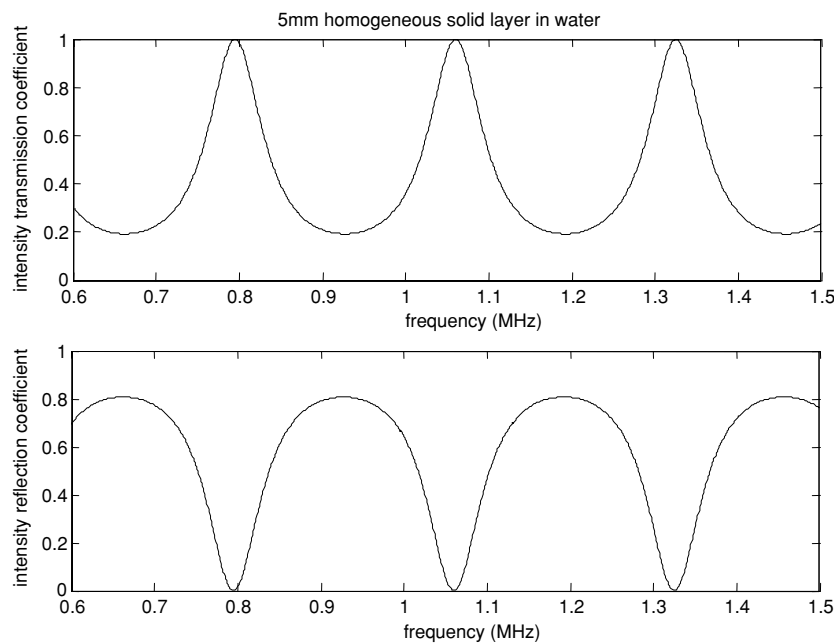


Figure 1. Transmission intensity coefficient (top) and the associated reflection intensity coefficient (bottom) for a 5 mm thick skull sample with parallel interfaces and a homogeneous mass density cross-section ($\rho = 2450 \text{ kg m}^{-3}$, $c = 2650 \text{ m s}^{-1}$).

of the skull, and hence, only longitudinal waves are actuated. In the frequency range of 0.6 MHz to 1.5 MHz, three local maxima in the simulated intensity transmission coefficient for a harmonic plane wave are observed to coincide in frequency with corresponding minima in the intensity reflection coefficient.

It was previously shown (Aarnio *et al* 2005) that the reflected signal from an impinging broadband pulse on the skull surface yielded a result similar to the reflection coefficient calculation of figure 1. From this spectral response, frequencies of maximum transmission are determined by the frequency of local minima in the intensity reflection coefficients.

To examine the implications of using this frequency optimization method with multiple ultrasound sources over the entire skull, this propagation model was modified to include a global frequency dependence, and then used with measured skull bone parameters. First, a quantitative analysis of skull thickness and mass density distribution was performed on a series of eight *ex vivo* human skulls. Mass density values were obtained by averaging computed tomographic (CT) Hounsfield values (Siemens, SOMATOM, AH82 inner ear kernel, 1 mm axial slices, 512×512 matrix, 200×200 mm field-of-view, 0.4 mm resolution) across the skull thickness and then extrapolating the mass density value using the Hounsfield values of water (1000 kg m^{-3}) and air (0 kg m^{-3}). Thickness values were calculated by threshold filtering to determine skull–water interfaces. The results obtained over 2484 points are presented in two histograms (figure 2). An average skull mass density value of 2132 kg m^{-3} and an average thickness of 6.1 mm were obtained from this analysis.

Frequency-dependent attenuation was then incorporated into the transmission model and the results were compared to the transmission spectrum from a sample point on a skull sample (measured data described in the materials and methods section). The model was calculated by combining a frequency-dependent attenuation factor (Connor *et al* 2002) with equation (1)

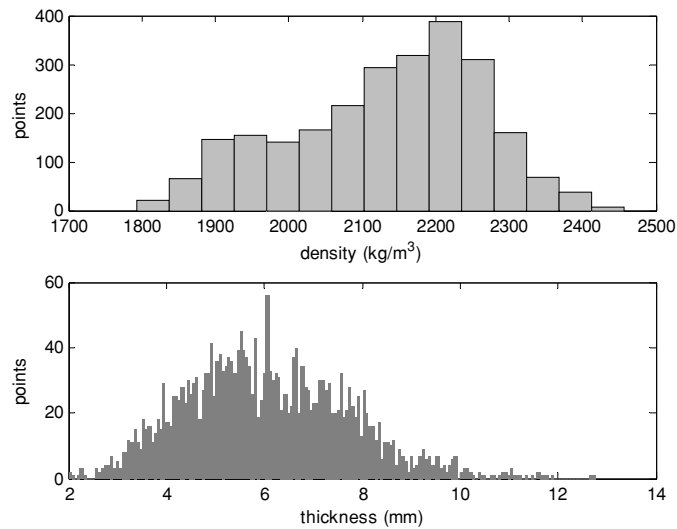


Figure 2. Thickness and mass density distribution for eight *ex vivo* human skulls over a total of 2484 points obtained from CT images. The mean measured mass density was 2132 kg m^{-3} with a standard deviation of 132 kg m^{-3} and the mean skull thickness was 6.1 mm with a standard deviation of 1.7 mm. Each bin in the upper histogram represents a span of 44.3 kg m^{-3} in density. Each bin in the lower histogram represents a span of 0.06 mm in thickness. (The bin sizes were chosen to correlate to a 10 kHz shift in the optimal frequency as measured from 1 MHz.)

such that

$$T = T_0 e^{-2\alpha d} \quad (3)$$

where $\alpha = -123 + 3.559 \times 10^{-4} f$ and d is the skull thickness. Mass density and thickness parameters from the analysis of CT data were used to generate a simulated transmission spectrum, which was then compared to experimental data. This model was then used to examine the effects of variations in mass density and thickness of the skull.

The superposition of single-frequency pressure waves that are temporally phase-matched will give a constructively-summed continuous wave of the same frequency. The superposition of pressure waves from multiple frequencies at a point in space will result in an intensity field that varies in time according to the differences in the frequencies of the combined pressure waves. To explore the effects of multiple-frequency superpositions in the context of frequency optimization, a simulation of the acoustic intensity at a single point produced by the summation of pressure waves from multiple sources was created. The simulation calculated and incorporated the transcranial transmission of different frequencies using mass density and thickness distributions from five skull specimens. The transmission spectra for a total of 1500 points divided among these specimens were modelled and the optimal transmission frequency peaks were chosen for comparison with the intensity transmission values at 0.7 MHz for each skull. The superposition of pressure values to obtain a time-varying acoustic pressure-squared value from N sources of optimal frequencies at one point in space was summed according to

$$p = \sum_{n=1}^N p_n e^{i(2\pi f_n t)} \quad (4)$$

where p_n is the peak pressure of the n th frequency. The result was compared with the same for the pressure-squared values at the single frequency of 0.7 MHz.

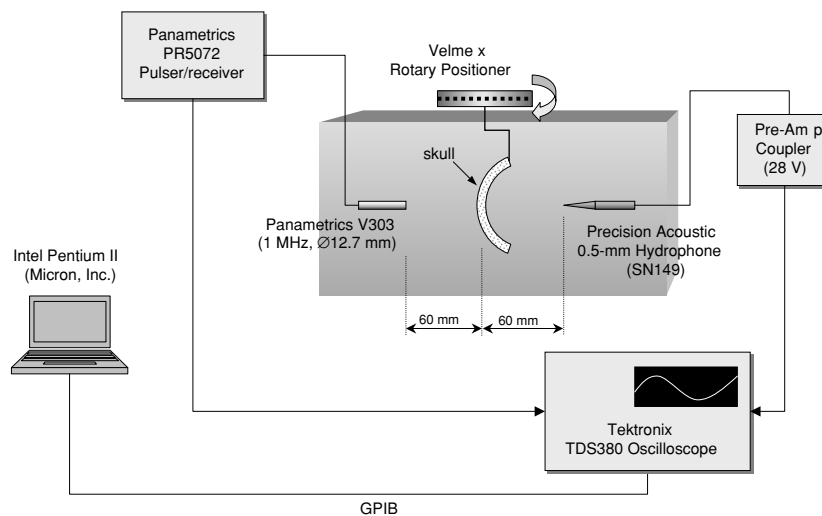


Figure 3. Experimental setup.

2.2. Experiments

Four *ex vivo* formalin-fixed human calvaria were submerged in degassed deionized water for experiments (figure 3). CT scans were performed for each specimen to aid in the analysis of results from the study and to ensure the absence of trapped gases within the *ex vivo* skull bone. Coronal and sagittal images were constructed from approximately 100 axial image slices per sample using a fast Fourier transform (FFT) interpolation technique with Matlab. With the aid of these reconstructed CT images, it was determined that, across the ultrasound beam width at the surface of the skull (-10 dB at a full width of 10.0 mm), the thickness varies by less than 0.3 ± 0.2 mm on average. The skulls were positioned approximately equidistant between a broadband planar transducer (-6 dB bandwidth = 60%, 0.97 MHz centre frequency, circular 12.7 mm diameter aperture) (Panametrics, Waltham, MA) and a polyvinylidene fluoride (PVDF) needle hydrophone (0.5 mm diameter aperture) (Precision Acoustics, Dorchester, UK). A total of 17 insonation points were selected by rotating the calvarium with a rotational stepping motor (Velmex, Bloomfield, NY) along the vertical axis as defined by the needle hydrophone measurement point (figure 4). All experiments were conducted in a tank with rubber-lined walls to minimize interference with reflected signals.

At each point, a broadband pulse generated by an ultrasound pulser-receiver (Panametrics, Waltham, MA, model V303) was transmitted and the reflected signal from the skull was received by the same transducer and recorded by a digital oscilloscope (Tektronix, Beaverton, OR, model TDS380) after 6 dB amplification. The waveform was then downloaded to a personal computer (PC) (Dell, Round Rock, TX) where a deconvolution of the transducer's impulse response was performed using Matlab (Mathworks, Natick, MA). The send-receive response of the transducer was obtained by recording the signal reflected from a water-air interface with the transducer face oriented parallel to and 60 mm from the surface. In addition, the portion of the same signal that transmits through the skull was sensed by the needle hydrophone, sent through a preamplifier (Precision Acoustics, Dorchester, UK), recorded by the oscilloscope, and downloaded to the PC. The impulse response of the transducer-hydrophone combination was obtained by transmitting the pulse unimpeded through water.

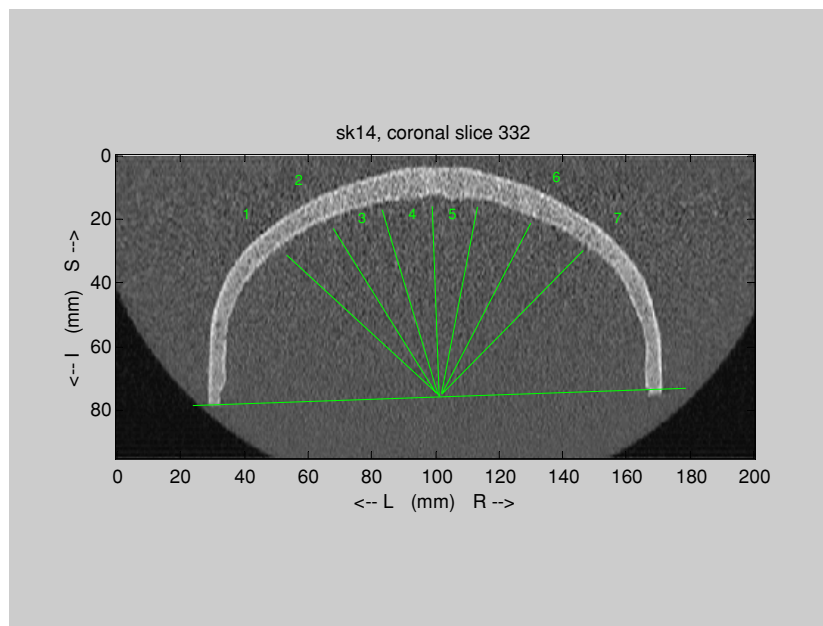


Figure 4. The superimposed rays on this CT image of an *ex vivo* human calvarium indicate the measurement points on each skull specimen as selected by rotation about the axis defined by the intersection of the anatomical midsagittal plane and the anatomical axial plane at the inferior extreme of the calvarium specimen.

For each insonated location on a skull, an analysis of the data was performed in which the ultrasound transmission at a frequency between two frequencies of maximum reflection peaks was compared to an expected transmission value based on a linear interpolation between the transmission values of the two flanking frequencies. Expectation values determined by linear interpolation, although not based on the physical principles of attenuation, yielded the worst-case results for transmission enhancement. The deviation from the expected value gave an indication as to whether acoustic power transmission was enhanced in a spectral region of diminished reflection.

In addition, the frequency shift between corresponding maxima of the reflection spectra and the minima of the transmission spectra were recorded for analysis. The local extrema of the reflection and transmission curves were obtained by locating the zeros of first derivatives with respect to frequency.

3. Results

3.1. Simulations

Using the CT-derived average skull thickness of 6.1 mm, an average mass density of 2132 kg m^{-3} (also from CT images) and a longitudinal sound speed of 2800 m s^{-1} (White 2005), the first two transmission peaks in the frequency range of 0.6 MHz to 1.4 MHz were calculated to be at 0.786 MHz and 0.983 MHz as compared to the peaks in the data (experimental results explained in more detail in the following section), which were at 0.764 MHz and 1.010 MHz (figure 5). This model was then used to determine the effects of mass density and thickness changes on the frequency dependence of the peaks in transmission. As shown in figure 6, a

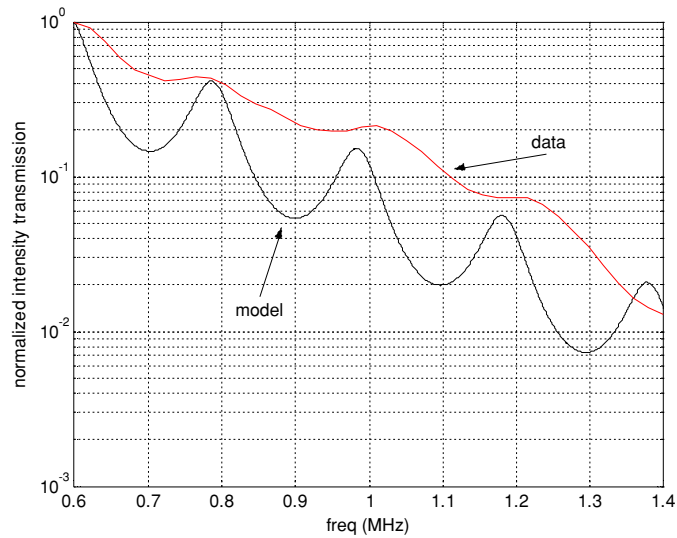


Figure 5. A propagation model of ultrasound transmission through a 6.1 mm homogeneous layer ($\rho = 2132 \text{ kg m}^{-3}$, $c = 2800 \text{ m s}^{-1}$) in water demonstrating correlation with the measured spectrum of transmission through an *ex vivo* calvarium.

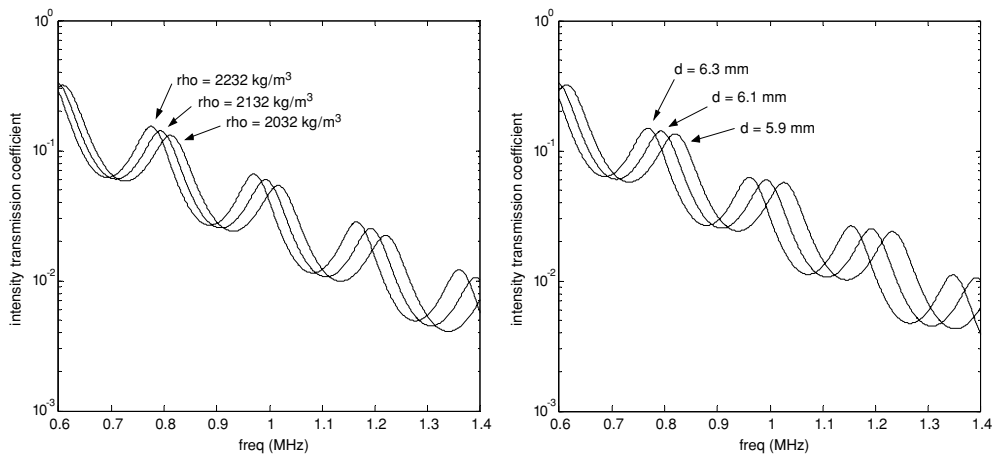


Figure 6. The calculated spectral dependence of ultrasound transmission on layer mass density and thickness. With increasing mass density and a constant thickness of 6.1 mm (left), a lowered optimal frequency was observed. With increasing layer thickness and a constant mass density of 2132 kg m^{-3} (right), a lowered optimal frequency was also observed.

21 kHz shift in a transmission peak from 1 MHz was calculated to arise from a 100 kg m^{-3} change in bone mass density. When the skull mass density was held constant, it was determined that a 33 kHz shift in a transmission peak from 1 MHz was the result of a 0.2 mm change in the skull thickness.

The transmission spectra for a total of 1500 points on five skull specimens were modelled and the optimal transmission frequency peaks were chosen for comparison with the intensity transmission values at 0.7 MHz for each skull (figure 7). The calculated time-averaged ultrasound pressure-squared value at one point for the multiple-frequency case was on average

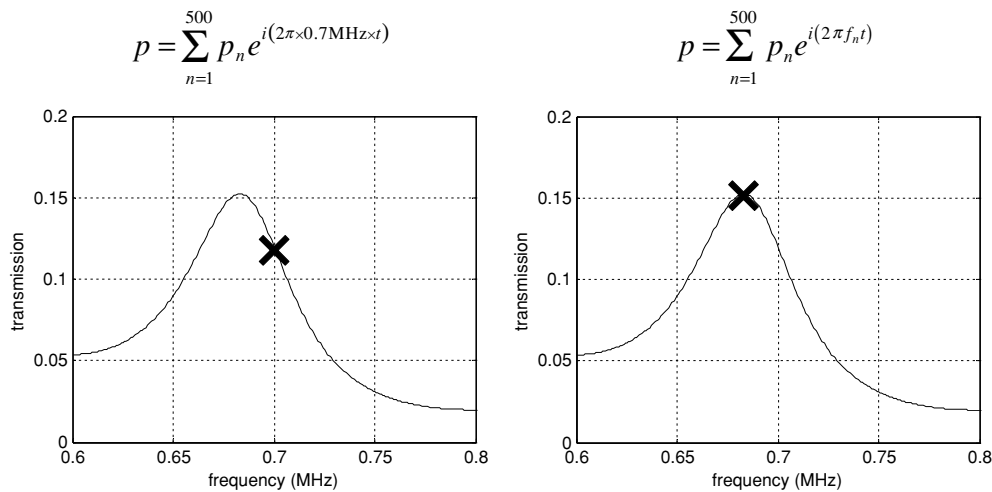


Figure 7. Schematic of the acoustic pressure summations performed for the scenarios of a single-frequency insonation (left) and a multiple-frequency insonation (right). The plots show simulated frequency-dependent intensity transmission coefficients.

$88 \pm 4\%$ lower than the same for the single-frequency case. As shown in figure 8, the instantaneous pressure-squared values for the multiple-frequency case (for one skull example) were observed to be substantially higher—by as much as 204% at the maximum—but only for a relatively brief time (above the single-frequency pressure-squared value for $4.0 \mu\text{s}$ every 1.3 ms). The periodicity of the transmission spikes was found to be directly related to the number of sources of differing frequencies, since phase coherence for n frequency-unique sources will only exist at a time interval equal to the reciprocal of the greatest-common-factor (GCF) of the n frequencies. As n , the number of frequencies, is increased, the GCF will either remain the same (highly unlikely, given the frequency range and resolution in this study) or will be decreased, and hence, in the latter case, yield a higher periodicity for phase-coherence spikes. Methods to modify the periodicity and duration of the transmission spikes would include changing n by altering the frequency range and resolution of frequency adjustments. Over all five skulls, the peak intensities averaged $230 \pm 20\%$ higher than the single-frequency pressure-squared values. So although frequency optimization yielded an increased transmission of energy for this point, the analysis demonstrated that this did not necessarily correspond to an overall increased time-average pressure-squared value at one point within the skull. It did, however, demonstrate that ephemeral higher peak values could be achieved with frequency optimization at the expense of an overall higher time-averaged pressure-squared at a single point in space. Thus, applications requiring large spatially localized time-averaged acoustic power levels may not benefit from this frequency optimization method whereas the temporary increased pressures resembling time-localized spikes could be useful for other applications.

3.2. Experiments

For the 17 insonation points on the four calvaria specimens, maxima and minima were observed in 15 of the reflected and transmitted acoustic power spectra in a pattern consistent with the predicted curves of figure 1 in that approximately three or four peaks were evident for the 0.6–1.4 MHz frequency range (figure 9). An analysis was performed to test the hypothesis

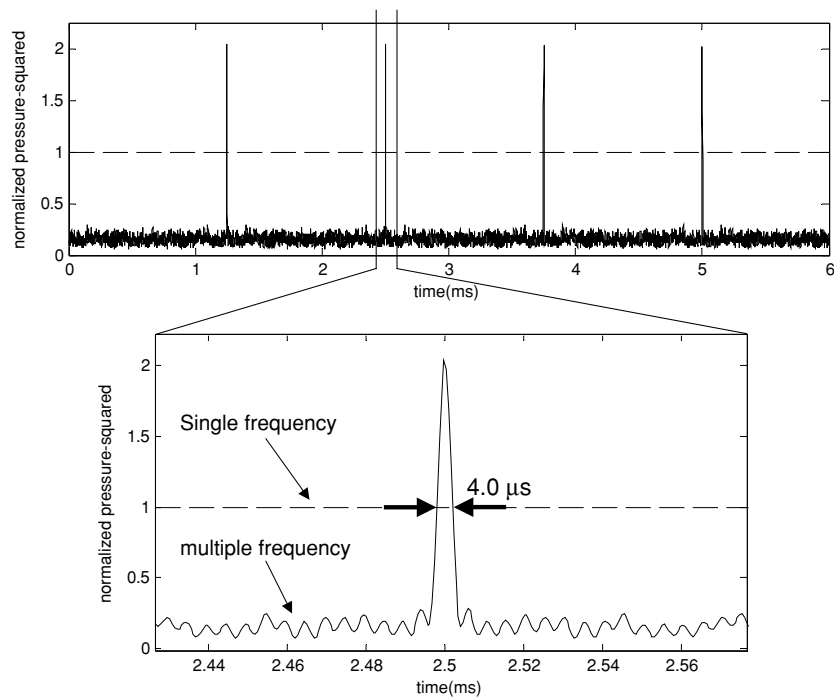


Figure 8. Time-dependent pressure-squared values at a single point in space calculated from the linear superposition of pressures from 500 sources of a single-frequency and the same from 500 sources of optimized frequencies. The time-averaged pressure-squared value for multiple-frequency superposition is 16% of that for the single-frequency case. This model was generated using calculated ultrasound transmission pressure-squared spectra. This calculation was performed for each of the 500 points on a skull specimen using the mass density and thickness distribution obtained from CT images. Five skulls were examined in this fashion.

that frequencies at which a peak in reflection is observed will transmit less acoustic power while the transmitted acoustic power will be enhanced with a insonation frequency that yields a dip in the reflection.

A comparison of transmission values was made using a linearly interpolated expectation between two selected reflection peaks from each insonation point based on the hypothesis that between two maxima in reflection, a local maximum in transmitted acoustic power will occur at the frequency of the local reflection minimum. Out of the 17 points, two were omitted from this analysis because only one reflection peak existed for their reflection spectra. The transmission values for the remaining 15 points were selected at two frequencies of distinct reflection. The transmission value for the frequency of minimum reflection between the two previously chosen frequencies was selected and compared to the expected value. The expected transmitted acoustic power for this frequency was determined by linearly interpolating between the two transmission values corresponding to the frequencies of maximum reflection. The deviation from the expected value indicated the level of transmission enhancement for ultrasound frequencies between those yielding maximum reflections. An 8% average increase in transmitted acoustic power was obtained by this analysis with a standard deviation of 26% (figure 10). The average change in transmitted acoustic power for each of the four skulls was calculated to be 16%, 2%, -18% and 34%.

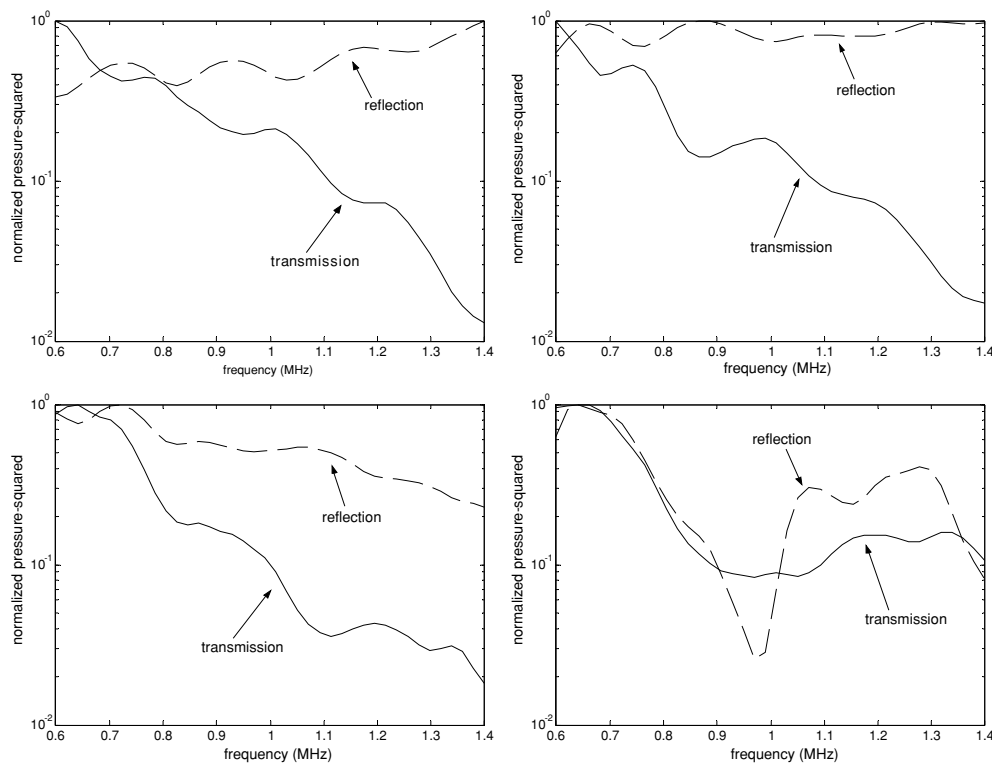


Figure 9. Normalized pressure-squared reflection spectra for four of the seventeen applied ultrasound pulses superimposed on the transmission spectra for the same points on the skull specimens. Each transmission and reflection signal was normalized to its own peak value. The four examples demonstrate, in clockwise sequence from the upper-left, insonations with progressively weaker correlations between dips in reflection values and peaks in transmission values.

To assess the accuracy in frequency alignment between the extrema of the reflection spectra and the transmission spectra, the variation in frequency was measured for each reflection minimum and its corresponding transmission peak; the same measurement was also performed for reflection peaks and their corresponding transmission minima. Over all the insonation points, the average frequency shift between reflection minima and their corresponding transmission peaks was 10 ± 30 kHz while, on average, there was no shift between the reflection peaks and their corresponding transmission minima.

4. Discussion

The results from this study gave evidence that ultrasound transmission through the human skull exhibits local fluctuations as a function of frequency in the range of 0.6 MHz to 1.4 MHz and that a pulse-reflection technique can give indications on the nature of these fluctuations. Overall, it was shown that frequencies of reflection peaks flank frequency regions where the transmission of ultrasound power will be on average 8% higher than an expected value given by linear interpolation. Yet, the results for each individual specimen revealed results that fluctuated from a 34% increase in transmitted power for one skull to a case where the transmission was reduced by 18% over the data points on one of the specimens. As shown

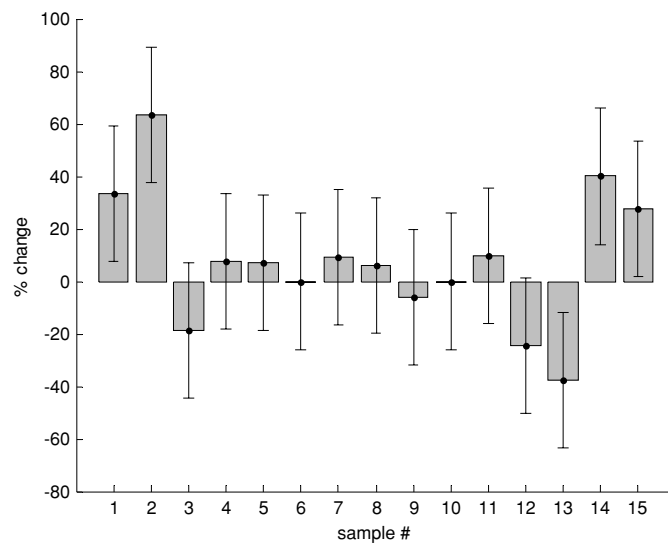


Figure 10. Percentage change in power transmission when insonating at an optimized frequency as determined by observation of the reflected ultrasound spectrum. Four of the fifteen cases demonstrated a decrease in power transmission.

in figure 9, the spectra for reflection and transmission at each point of the skull can yield results with a high degree of correlation between the extrema of the two curves, but in some cases the correlations are substantially weaker. Since this variation in results is likely due to inhomogeneities in the structure of skull bone and the non-parallelism between the inner and outer surfaces, this method to determine optimal frequencies may be fundamentally limited by the constraints of anatomical parameters.

With further analysis and simulations, it was demonstrated that the time-varying nature of combining pressure waves of multiple frequencies at one point in space yielded time-localized increases yet an overall decrease in the pressure-squared value due to destructive interference. The effects of frequency optimization over a substantial volume in space would require more extensive studies and experiments.

Acknowledgments

This work was supported by grant R01EB003268 and [U41RR019703](#) from the National Institutes of Health.

Appendix

Given a one-dimensional harmonic plane wave in epicranial tissue (which was approximated as a fluid in this study) that impinges on the skull surface at normal incidence (both skull interfaces are approximated to be planar and parallel, and the skull matrix is assumed to be an elastic non-fluid layer, which is also homogenous and non-absorbing), the incident pressure is defined as

$$p_{if} = A e^{j(\omega t - k_f x)} \quad (\text{A.1})$$

where the subscript i denotes an incident pressure, the subscript f indicates that the wave is propagating in a fluid, A is the peak-to-peak amplitude, ω is the angular frequency, t is the time variable, k_f is the wave number in the fluid and x is the spatial variable which is normal to the interfaces of the skull. A portion of this wave is transmitted into the skull bone while the remainder is reflected back into the fluid. The reflected wave is given as

$$p_{rf} = B e^{j(\omega t + k_f x)}. \quad (\text{A.2})$$

The transmitted wave,

$$p_{tb} = C e^{j(\omega t - k_b x)} \quad (\text{A.3})$$

is propagated through the bone and impinges on the inner surface, from where two more waves are then generated: for parallel interfaces, a reflected wave back into the bone of the form

$$p_{rb} = D e^{j(\omega t + k_b x)} \quad (\text{A.4})$$

and a wave that is transmitted into the brain

$$p_{tf} = E e^{j(\omega t - k_f x)}. \quad (\text{A.5})$$

In equations (A.2)–(A.5), the subscript r is used to denote a reflected wave while the subscript b indicates that the propagation medium is bone. The theory assumes the same acoustic parameters for the epicranial tissue and the brain matrix (i.e. $k_f = k_{f1} = k_{f2}$). Continuity of normal specific acoustic impedances at the boundaries gives

$$\frac{A + B}{A - B} = \frac{(\rho c)_b}{(\rho c)_f} \frac{C + D}{C - D} \quad (\text{A.6})$$

and

$$\frac{C e^{-jk_b d} + D e^{jk_b d}}{C e^{-jk_b d} - D e^{jk_b d}} = \frac{(\rho c)_f}{(\rho c)_b} \quad (\text{A.7})$$

where d is the thickness of the skull at the point of transmission. Defining the pressure reflection coefficient (\mathbf{R}) of this entire system as the ratio between the reflected pressure and the incident pressure, the following expression is obtained from equations (A.6) and (A.7):

$$\mathbf{R} = \frac{p_{rf}}{p_{if}} = \frac{j \left[\frac{(\rho c)_b}{(\rho c)_f} - \frac{(\rho c)_f}{(\rho c)_b} \right] \sin k_b d}{2 \cos k_b d + j \left[\frac{(\rho c)_b}{(\rho c)_f} + \frac{(\rho c)_f}{(\rho c)_b} \right] \sin k_b d}. \quad (\text{A.8})$$

Using the definition $T = 1 - |\mathbf{R}|^2$, the intensity transmission coefficient becomes

$$T = \frac{1}{1 + \frac{1}{4} \left[\frac{(\rho c)_b}{(\rho c)_f} - \frac{(\rho c)_f}{(\rho c)_b} \right]^2 \sin^2 k_b d}. \quad (\text{A.9})$$

From equation (A.9) it is evident that at frequencies such that $k_b d = n\pi$, the intensity transmission coefficient becomes unity, leading to null reflection intensity coefficients at those same frequencies.

References

- Aarnio J, Clement G T and Hynynen K 2005 A new ultrasound method for determining the acoustic phase shifts caused by the skull bone *Ultrasound Med. Biol.* **31** 771–80
- Behrens S, Spengos K, Daffertshofer M, Schroeck H, Dempfle C E and Hennerici M 2001 Transcranial-ultrasound-improved thrombolysis: diagnostic versus therapeutic ultrasound *Ultrasound Med. Biol.* **27** 1683–9
- Carson P L, Oughton T V, Hendee W R and Ahuja A S 1977 Imaging soft tissue through bone with ultrasound transmission tomography by reconstruction *Med. Phys.* **4** 302–9

- Cheeke J D N 2002 Reflection and transmission of ultrasonic waves at interfaces *Fundamentals and Applications of Ultrasonic Waves* (Boca Raton, FL: CRC Press) pp 115–42
- Clement G T, Sun J, Giesecke T and Hynynen K 2000 A hemisphere array for non-invasive ultrasound brain therapy and surgery *Phys. Med. Biol.* **45** 3707–19
- Connor C, Clement G T and Hynynen K 2002 A unified model for the speed of sound in cranial bone based on genetic algorithm optimization *Phys. Med. Biol.* **47** 3925–44
- Daum D R, Buchanan M T, Fjield T and Hynynen K 1998 Design and evaluation of a feedback based phased array system for ultrasound surgery *IEEE Trans. Ultrason. Ferroelectr. Freq. Control* **45** 431–8
- Dines K A, Fry F J, Patrick J T and Gilmor R L 1981 Computerized ultrasound tomography of the human head: experimental results *Ultrason. Imaging* **3** 342–51
- Fry F J 1977 Transkull transmission of an intense focused ultrasonic beam *Ultrasound Med. Biol.* **3** 179–84
- Fry F J, Eggleton R C and Heimburger R F 1974 Transkull visualization of brain using ultrasound: an experimental model study *Excerpta Medica* 97–103
- Hynynen K and Jolesz F A 1998 Demonstration of potential noninvasive ultrasound brain therapy through an intact skull *Ultrasound Med. Biol.* **24** 275–83
- Hynynen K, McDannold N, Vykhodtseva N and Jolesz F A 2001 Noninvasive MR imaging-guided focal opening of the blood-brain barrier in rabbits *Radiology* **220** 640–6
- Kinsler L E, Frey A R, Coppens A B and Sanders J V 2000 Reflection and transmission *Fundamentals of Acoustics* 4th edn (New York: Wiley) pp 149–71
- Kirkham F J, Padayachee T S, Parsons S, Seargeant L S and House F R 1986 Transcranial measurement of blood flow velocities in the basal cerebral arteries using pulsed Doppler ultrasound *Ultrasound Med. Biol.* **12** 15–21
- Lynn J G, Zwemer R L, Chick A J and Miller A E 1942 A new method for the generation and use of focused ultrasound in experimental biology *J. Gen. Physiol.* **26** 179–93
- Postert T, Hoppe P, Federlein J, Przuntek H, Buttner T, Helbeck S, Ermert H and Wilkening W 2000 Ultrasonic assessment of brain perfusion *Stroke* **31** 1460–2
- Smith S W, Phillips D J, von Ramm O T and Thurstone F L 1979 Some advances in acoustic imaging through the skull *Nat. Bur. Standards Pub. no 525* pp 209–18
- Sun J and Hynynen K 1999 The potential of transskull ultrasound therapy and surgery using the maximum available skull surface area *J. Acoust. Soc. Am.* **105** 2519–27
- Tanter M, Thomas J L and Fink M 1998 Focusing and steering through absorbing and aberrating layers: application to ultrasonic propagation through the skull *J. Acoust. Soc. Am.* **103** 2403–10
- Thomas J and Fink M A 1996 Ultrasonic beam focusing through tissue inhomogeneities with a time reversal mirror: application to transskull therapy *IEEE Trans. Ultrason. Ferroelectr. Freq. Control* **43** 1122–9
- Tobias J, Hynynen K, Roemer R, Guthkelch A N, Fleischer A S and Shively J 1987 An ultrasound window to perform scanned, focused ultrasound hyperthermia treatments of brain tumors *Med. Phys.* **14** 228–34
- White P J 2005 Modalities for the optimization of ultrasound transmission through the human skull *PhD Thesis* Pennsylvania State University
- Ylitalo J, Koivukangas J and Oksman J 1990 Ultrasonic reflection mode computed tomography through a skull bone *IEEE Trans. Biomed. Eng* **37** 1059–66